NANO LETTERS
Letter
Cite This: Nano Lett. 2019, 19, 1−7
pubs.acs.org/NanoLett

# In Vitro Monitoring Conformational Changes of Polypeptide Monolayers Using Infrared Plasmonic Nanoantennas

Rostyslav Semenyshyn,[†,‡] Mario Hentschel,[†,‡] Christoph Stanglmair,[§] Tanja Teutsch,[∥] Cristina Tarin,[∥] Claudia Pacholski,[§,⊥] Harald Giessen,[†,‡] and Frank Neubrech*[,†,#]

[†]4th Physics Institute and Research Center SCoPE, University of Stuttgart, Pfaffenwaldring 57, 70569 Stuttgart, Germany
[‡]Center for Integrated Quantum Science and Technology, IQST, Pfaffenwaldring 57, 70569 Stuttgart, Germany
[§]Max Planck Institute for Intelligent Systems, Heisenbergstraße 1, 70569 Stuttgart, Germany
[∥]Institute for System Dynamics, University of Stuttgart, Waldburgstraße 17/19, 70563 Stuttgart, Germany
[⊥]Institute of Chemistry, University of Potsdam, Am Mühlenberg 3, 14476 Potsdam OT Golm, Germany
[#]Kirchhoff Institute for Physics, University of Heidelberg, Im Neuenheimer Feld 227, 69120 Heidelberg, Germany

Supporting Information

**ABSTRACT:** Proteins and peptides play a predominant role in biochemical reactions of living cells. In these complex environments, not only the constitution of the molecules but also their three-dimensional configuration defines their functionality. This so-called secondary structure of proteins is crucial for understanding their function in living matter. Misfolding, for example, is suspected as the cause of neurodegenerative diseases such as Alzheimer's and Parkinson's disease. Ultimately, it is necessary to study a single protein and its folding dynamics. Here, we report a first step in this direction, namely ultrasensitive detection and discrimination of in vitro polypeptide folding and unfolding processes using resonant plasmonic nanoantennas for surface-enhanced vibrational spectroscopy. We utilize poly-L-lysine as a model system which has been functionalized on the gold surface. By in vitro infrared spectroscopy of a single molecular monolayer at the amide I vibrations we directly monitor the reversible conformational changes between $\alpha$-helix and $\beta$-sheet states induced by controlled external chemical stimuli. Our scheme in combination with advanced positioning of the peptides and proteins and more brilliant light sources is highly promising for ultrasensitive in vitro studies down to the single protein level.

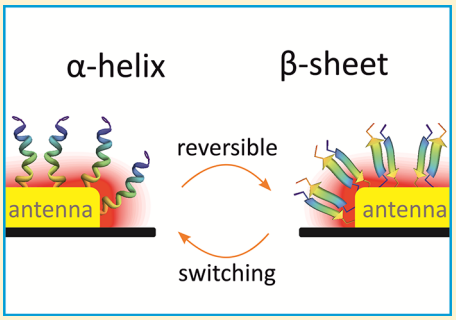


**KEYWORDS:** *Plasmonics, surface-enhanced infrared absorption spectroscopy, proteins, conformational changes, biosensing*



Biological and physiological processes take place in three dimensions. The three-dimensional conformation of the involved biomolecules such as proteins is key for understanding their working principle. Due to their very large sizes, most of these molecules can fold in several distinct configurations, which is termed secondary structure of molecules. The interaction of individual molecules during biological and physiological processes is thus greatly influenced by their conformation which is complementary to their molecular constitution. Understanding the interactions in living matter is therefore directly linked to understanding the conformation and the conformational changes of the associated molecules during their interaction. For instance, misfolding of disease-related proteins is considered to play a crucial role in incurable diseases such as Alzheimer's, Huntington's, and Parkinson's diseases.[1,2]

The secondary structure of molecules is difficult to determine as the composition of the molecule in its distinct conformations is identical. Different techniques have been used and proposed, including circular dichroism spectroscopy (CD),[3,4] nuclear magnetic resonance (NMR) spectroscopy,[5−7] X-ray crystallography,[8,9] atomic force microscopy (AFM),[10,11] and nanopore diffusion[12] studies. The continued quest for additional strategies despite the apparent plethora of techniques is related to inherent drawbacks: CD, NMR, and X-ray crystallography require large amounts of analyte, a number of techniques, such as AFM, cannot be performed in vitro, additionally real-time observations might even be impossible. However, unraveling the structural transition pathways would be possible with label-free single molecule sensitivity and in vitro studies, ideally with real time resolution.

Vibrational spectroscopy, i.e., Raman and infrared spectroscopy, is a powerful method to identify particular conformations of molecules.[13−15] The multitude of bonds in the molecules leads to a large set of vibrational excitations, that is, the oscillation of individual atoms with respect to each other. Each of these vibrations has a characteristic resonance frequency

Received: June 12, 2018
Revised: July 27, 2018
Published: August 2, 2018




DOI: 10.1021/acs.nanolett.8b02372
Nano Lett. 2019, 19, 1−7

which causes a distinct vibrational fingerprint of a molecule, enabling label-free detection of molecular species. As the vibrations are also influenced by their respective surrounding, including peptide-bond angles and hydrogen-bonding patterns, these frequencies are also subject to changes during conformational transitions.[16−20] Thus, a molecule in its different conformational states has distinct vibrational spectra despite an identical chemical formula. This also allows monitoring of the conformational changes of molecules during physiological processes. This information is complementary to the mapped conformation as the transition from one state to another provides important information about the reaction pathways. This transition pathway, i.e., the exact intermediate states during folding and unfolding of the molecules, can offer insight into the working principle of the underlying processes.

Classical vibrational spectroscopy, similarly to the aforementioned techniques, requires large amounts of molecules in order to obtain a sufficient signal-to-noise ratio. Studying individual molecules or even the interaction of molecules with one another and the associated changes to the three-dimensional arrangement is thus virtually impossible. This limitation can be lifted by surface enhanced infrared spectroscopy (SEIRA). Here, the locally enhanced electric fields of metallic nanostructures are used to enhance the infrared vibrational modes of molecules. In the past, films of randomly distributed metal islands of various shapes and sizes were applied to study protein dynamics including conformational changes.[21−23] However, chip-level based resonant SEIRA,[24−27] where the resonance frequency of the plasmonic mode and the molecular vibrational absorption are perfectly matched, provides a much higher sensitivity[21] compared to the conventional SEIRA approach. This higher sensitivity, together with more stable light sources, will in the future also allow for time-dependent measurements. It enables the detection of minute amounts of molecules on the plasmonic structures with attomolar sensitivity.[28,29] Rod antenna arrays were already successfully used for biosensing in air[11,30−34] as well as aqueous surroundings,[35−37] demonstrating the reliable detection of even submonolayers of molecules. These experiments gave detailed information about the near-field distribution of light fields around the nanoantennas and their interaction with the vibrational resonances of the molecules.[24,28,38] Adapting this technique, it became possible to detect the preset conformation of biomolecules in aqueous surrounding.[39] However, the in vitro *monitoring* of reversible conformational changes, namely, the cyclic transition from one conformation to another and back, of a single molecular monolayer has not yet been demonstrated.

In this work, we report for the first time the application of resonant surface enhanced infrared absorption spectroscopy for in vitro monitoring of structural changes of a molecular monolayer of polypeptides, here poly-L-lysine (PLL). Figure 1 illustrates the basic idea behind our setup. Standard Fourier-Transform (FT)-IR spectroscopy is used to probe the optical response of resonant plasmonic nanoantennas in inverse reflection geometry. The antennas are immersed in an aqueous environment (Figure S1 in the Supporting Information) and functionalized with a monolayer of poly-L-lysine molecules. Poly-L-lysine has been chosen for two reasons: On the one hand, it is a widely used polypeptide in biological applications, such as the functionalization of surfaces or sensors. On the other hand, poly-L-lysine can be well controlled and functionalized, which are crucial prerequisites in our experimental

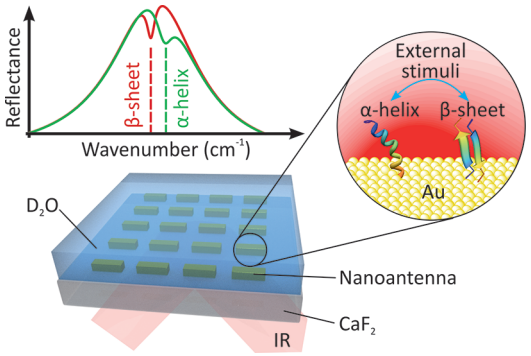


**Figure 1.** Chip-level based SEIRA for in vitro monitoring of conformational changes of polypeptides. A monolayer of poly-L-lysine (PLL) as a model system for polypeptides is immobilized in the plasmonic hotspots of gold (Au) nanoantennas. The amide vibration of PLL is enhanced if the plasmon is resonantly matched to the molecular vibration. By adding external stimuli, the secondary structure can be reversibly changed from the $\alpha$ to the $\beta$ state resulting in different substructures of the amide vibration. The experiments are performed in aqueous solution.

scheme. Chemical stimuli are used to switch the secondary structures of polypeptides ($\alpha$-helix or $\beta$-sheet state) and thus leave the system in a defined state. During the transition, the defined and known states are then optically probed, allowing us to monitor the induced conformational changes. The recorded optical spectra will thus display the characteristic vibrational features of the two specific conformations (i.e., the substructure of the amide vibrations), allowing us to determine the secondary structure from the optical response alone.

As a first step, we characterized the utilized poly-L-lysine and its properties (Figure S2 in the Supporting Information). Poly-L-lysine is a water-soluble polypeptide composed of naturally occurring L-lysine, which contains amine groups on the side chains. PLL can be found in three distinct conformations, $\alpha$-helix, $\beta$-sheet, and random coil (as well as mixtures). The secondary structure is determined by the external environment (e.g., solvents and temperatures) and can thus be switched at will, an important prerequisite for our experiments. It has been shown that conformational transitions can be induced by various external stimuli, including heat,[18] pH,[22,40,41] alcohol,[41] solvents,[42] and surfactants.[43,44] In contrast to previous studies, we strive to observe the folding and unfolding of PLL, ideally the cyclic transition between $\alpha$-helix and $\beta$-sheet states. Consequently, not all of the aforementioned stimuli are suitable as in some cases the stimulation causes permanent denaturation. Therefore, we focus on folding-unfolding of PLL induced by surfactants, namely sodium dodecyl sulfate (SDS) as well as by variation of the external basicity level. The recipe of SDS solution we used was introduced previously in the literature.[43]

As mentioned above, molecules exhibit characteristic vibrational spectra in the IR spectral range. In our case, the amide-I band resulting from backbone vibrations[45] will be monitored to assign the secondary structures to poly-L-lysine. In the $\alpha$-helical conformation the amide vibration peaks at 1644 $cm^{-1}$ and at 1618 $cm^{-1}$ in the $\beta$-sheet state.[17] As $H_2O$ exhibits vibrational fingerprints in the amide-I spectral range, we utilized $D_2O$ featuring vibrational features at lower energies as a solvent in order to circumvent this parasitic $H_2O$ absorption. We are therefore not tuning the pH level but rather the pD levels. To reduce the $D_2O$ absorption in our


DOI: 10.1021/acs.nanolett.8b02372
Nano Lett. 2019, 19, 1−7

experiments, a specially designed transmittance flow cell and an inverse reflection setup probing $\mu$L volumes of solution were used. All IR spectra were taken in transmission (bulk solution) or inverse reflection geometry (SEIRA measurements) with a standard FTIR microscope on specifically designed resonant plasmonic nanoantenna arrays (see the Supporting Information).

As we are going to enhance the vibrational signal utilizing resonant plasmonic nanoantennas we need to controllably place the polypeptides inside the local electric field around the nanostructures. This task is accomplished by a functionalization scheme, which is sketched in Figure 2a. Two points are of great importance: On the one hand, the polypeptides need to be attached to the antennas close enough to the surface as to interact with the local electric field.[30,46] On the other hand, the polypeptides need to be at a large enough distance to the surface as well as to their neighboring polypeptides in order to be able to undergo the desired structural transitions.[22] We use two types of thiols, namely 11-mercaptoundecanoic acid (MUA) and 11-mercaptoundecanol (MUoL) for the antenna functionalization. These bind to the gold antennas and not the surrounding $CaF_2$ and provide the required larger surface-polypeptide-distance as well as the lateral spacing. To predispose the carboxyl group of MUA for the binding to the poly-L-lysine an EDC/NHSS (*N*-(3-(dimethylamino)-propyl)-*N*′-ethylcarbodiimide hydrochloride, *N*-hydroxysulfosuccinimide sodium salt) solution in MES (2-(*N*-morpholino)-ethanesulfonic acid) buffer is used. For further details, please refer to the Supporting Information and ref 22, where the recipe is introduced and the role of MUoL is discussed as well.

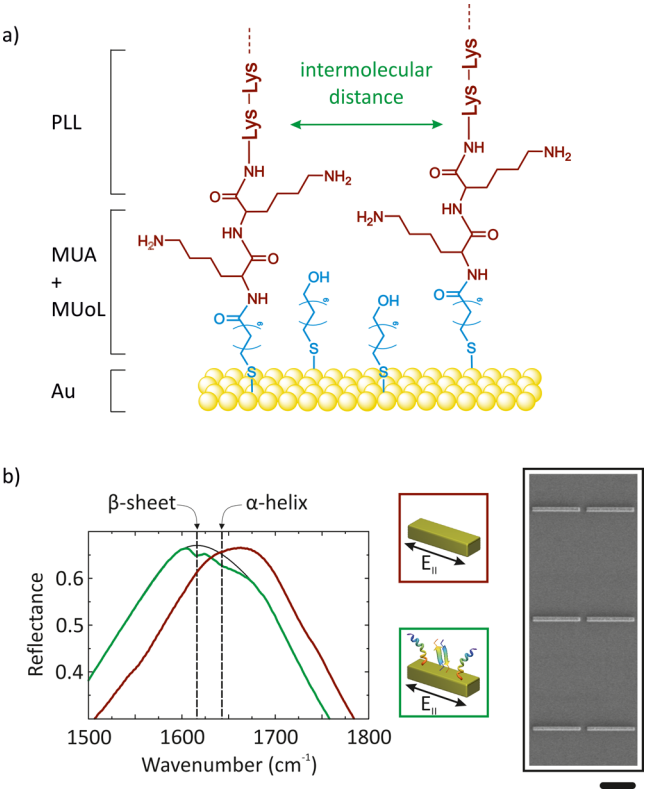


**Figure 2.** IR optical properties of the poly-L-lysine model system and functionalization scheme. (a) PLL molecules are immobilized on a gold surface using a mixed monolayer of MUA and MUoL. The intermolecular distance between PLL molecules, which can be adjusted by the composition of MUA/MUoL, and their distance to the gold surface are crucial for conformational changes. (b) Reflectance spectra of resonant nanoantenna arrays in $D_2O$ are taken before (red) and after (green) functionalization with MUA/MUoL and poly-L-lysine (see illustrations). After molecular adsorption, the resonance frequency is shifted, and the amide I vibration is enhanced by the plasmonic nearfields. The SEM image depicts an exemplary antenna array; the scale bar is 1 $\mu$m.

The gold nanoantenna arrays (100 $\mu$m × 100 $\mu$m) were produced by standard electron beam lithography in a positive tone resist (PMMA) via lift-off. Such top-down techniques offer the possibility to tailor the geometry and properties of the antennas at will and such optimize their performance according to the needs of our experiment. A number of issues are important here, namely the strength of the local field enhancement and the Rayleigh anomalies,[30] as well as the geometrical access of the polypeptides to the nanoantennas, i.e., the spacing and gap size between adjacent nanostructures. Taking into account these points, we varied the length of the nanoantennas between 1350 and 1750 nm with a lateral spacing of constant 200 nm in the *x*-direction (along the long antenna axis) and a period of 3300 nm in the *y*-direction (along the short antenna axis). The antennas width and height are fixed at 100 nm. Titanium was used as an adhesion layer on the IR transparent $CaF_2$ substrates due to its chemical stability at large pD levels.

Figure 2b depicts the measured spectra of one exemplary nanoantenna array with an antenna length of 1500 nm acquired in an inverse reflection geometry. The red curve shows the response of the unfunctionalized antenna array inside the flow cell filled with $D_2O$. A pronounced plasmonic resonance can be observed for light polarized along the antenna axis at about 1650 $cm^{-1}$, nearly perfectly matched to the energies of the vibrational modes which are expected at 1644 and 1618 $cm^{-1}$ (see Figure S3 and Figure S4 in the Supporting Information for further information). After the functionalization with MUA/MUoL and poly-L-lysine, the sample was rinsed and placed in the flow cell filled with $D_2O$. It is important to note that during this process the sample is always in aqueous environment. We observe two distinct differences: The plasmonic resonance undergoes a spectral redshift which is caused by the larger effective refractive index of the surrounding due to the deposition of the functionalization layer and poly-L-lysine. Additionally, we clearly observe two vibrational features imprinted on the plasmonic resonance. These features come about due to the coupling of the vibrational modes to the plasmonic resonance. In order to extract the enhanced vibrational signal strength, which is a measure of the number of polypeptides in a certain conformation, we need to perform a baseline correction. The baseline characterizes the plasmonic response in the absence of the vibrational modes and is calculated from the coupled system using an adapted version of the asymmetric least-squares smoothing algorithm proposed by Eilers[47] and is shown in black. Subtracting this baseline from the measured spectra delivers the so-called baseline-corrected vibrational spectra.

Figure 3 depicts our main findings and shows the cyclic folding and unfolding of a single monolayer of poly-L-lysine under external chemical stimuli. The left side shows a sketch of the nanoantenna as well as the conformation of the polypeptides. Again, it is important to stress that we are able to reliably and controllably set the conformation of the


DOI: 10.1021/acs.nanolett.8b02372
Nano Lett. 2019, 19, 1−7

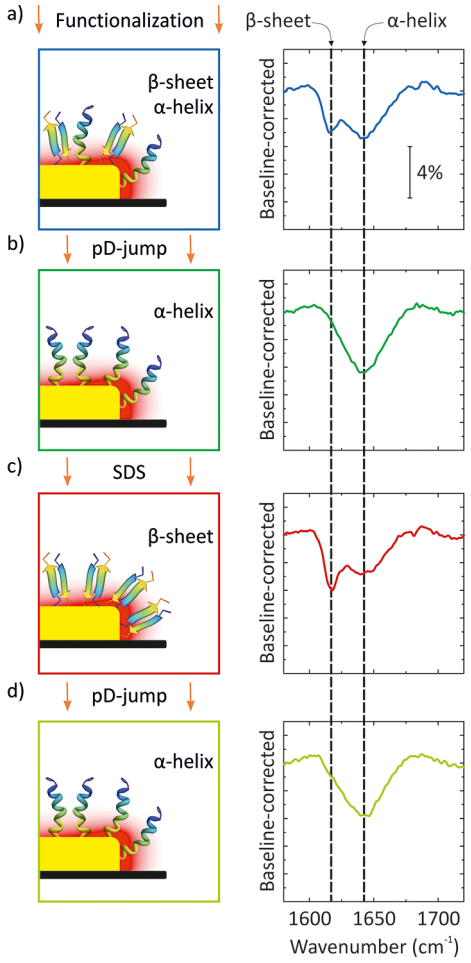


**Figure 3.** In vitro monitoring of PLL conformational changes. Baseline-corrected SEIRA signals (right) of nanoantennas functionalized with PLL under different external stimuli. (a) After functionalization, PLL molecules are in a random mixture of $\alpha$-helix to $\beta$-sheet as evidenced by the vibrational substructure of the amide band. (b) If the basicity is increased to a pD-value of 12, the vibrational signature of the $\beta$-sheet state (1618 $cm^{-1}$) vanishes, and only the $\alpha$-helix state (1644 $cm^{-1}$) signature remains. (c) SDS forces a transition of the polypeptides back to the $\beta$-sheet state. (d) A second increase in basicity (pD of 12) switches the vast majority of molecules back to the $\alpha$-helix state. The vertical dashed lines indicate amide vibration of PLL in the $\alpha$-helix and $\beta$-sheet states.

polypeptides by an external stimulus. This information serves as a benchmark for the vibrational fingerprints we are retrieving from our measurements. The baseline-corrected vibrational features, which are imprinted on the spectrum of the functionalized antennas, are displayed in the right column. Panel (a) of Figure 3 shows the response right after functionalization. As discussed earlier, the polypeptides are now in a random distribution of $\alpha$-helical and $\beta$-sheet states. The measured spectra reflect this known behavior. The baseline-corrected spectrum exhibits the vibrational signatures of the of $\alpha$-helical and $\beta$-sheet states at 1644 and 1618 $cm^{-1}$, respectively. We now perform a pD-jump from 7 to 12 which is known to force the polypeptides into the $\alpha$-helical state,[18] shown in panel (b) of Figure 3. As expected, the signature of the $\beta$-sheet state vanishes from the vibrational spectrum, clearly showing a near-unity $\alpha$-helical state distribution. We now exchange the solution in our flow cell with an SDS solution which switches the poly-L-lysine to the $\beta$-sheet conformational state, depicted in panel (c) of Figure 3. In the vibrational spectrum we observe the reappearance of the $\beta$-sheet vibrational feature at 1618 $cm^{-1}$. However, the fingerprint at 1644 $cm^{-1}$ associated with the $\alpha$-helical state remains, yet significantly weaker. This result indicates that only part of the polypeptides folds back into the $\beta$-sheet state, while some remains in the $\alpha$-helical conformation, as seen in ensemble measurements (Figure S2). A further and final pD jump should again force all polypeptides in the $\beta$-sheet state back to the $\alpha$-helical one. The vibrational spectrum shown in panel (d) of Figure 3 now indeed exhibits the mode solely at 1644 $cm^{-1}$ indicating again a near-unity $\alpha$-helical state distribution. The same results were obtained for antenna arrays of other lengths, see Figure S5 in the Supporting Information.

To quantify the performance of our approach, we estimated the number of molecules contributing to the enhanced fingerprints, which are located in the area of the nanoantenna tip ends.[48] Based on this and on the assumption of a spherical PLL molecule with a diameter of roughly 4 nm,[49,50] we estimate the number to be about 1600 PLL molecules per antenna which contribute to the enhanced signal.

In order to further analyze the data and to support our interpretation without performing a baseline correction, we applied principal component analysis (PCA) on the raw data, which contain 200 individual spectra in total (50 for each external stimulus). PCA is a common method in multivariate statistics, which extracts the correlation of data points by applying a principal axis transformation such that the variance of the data sets becomes maximum.[51] Appropriate calibration measurements even allow extracting concentration ratios.[52]

Applying PCA to our data, we can express each spectrum $i$ ($i \in [1,200]$) as

$$\text{Spectrum}_i = A + \sum_{j=1}^{200} (k_{i,j} \cdot \text{PC}_j)$$

where $A$ is the average taken over all 200 spectra. The principal components $PC_j$ are therefore correction spectra to the average experimental spectrum. The principle components are the same for all 200 experimental spectra, whereas the weighting coefficients $k_{i,j}$, also called scores of principle component $j$, are related to the spectrum $i$. In the present study, only the first and second principle component are of relevance (see the Supporting Information). It is important to note that the principle components do not have an a priori interpretation or meaning. However, the principle components are expected to express the physical processes in our system, that is, the folding and unfolding of the proteins, among other influences.

Figure 4a depicts the first and the second principal components. The first principle component, interestingly, exhibits hardly any spectral features but is nearly flat over the entire spectral range. When inspecting the different measured spectra (see Figure S7 in the Supporting Information) we observe a clear intensity drift in the magnitude of the plasmon resonance. This drift is linked to experimental challenges in stabilizing the setup over hours of data acquisition. We thus conclude that the first principle component captures this drift and only shifts the absolute value of the spectra. Therefore, it does not contain any information about the protein folding dynamics. The observed intensity drift in the experimental spectra, which is captured in the first PC, can also be removed before applying PCA, which is shown


DOI: 10.1021/acs.nanolett.8b02372
Nano Lett. 2019, 19, 1−7

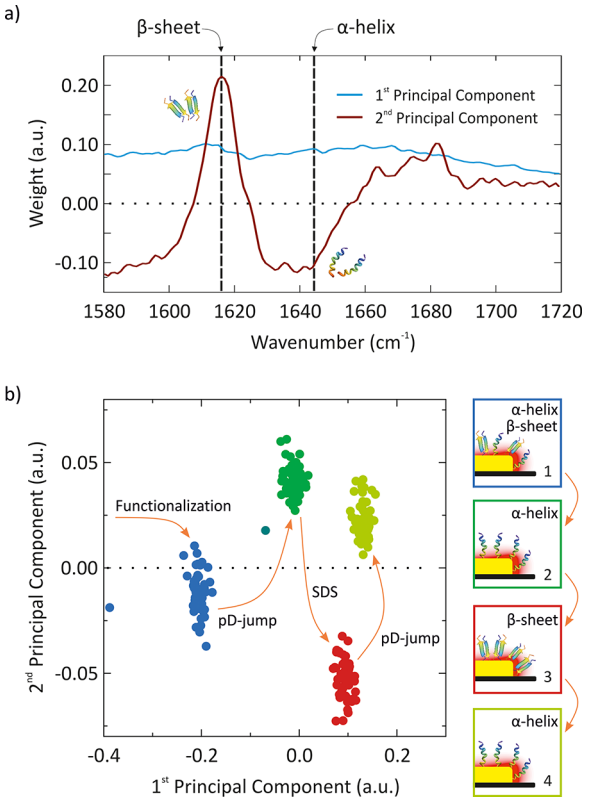


**Figure 4.** Principal component analysis (PCA) of PLL structural changes. The first and second principal components and their scores are determined. (a) The first principal component resembles intensity changes of the resonantly scattered light. The second principal component represents the changes of molecular vibration under the external chemical stimuli. Most of the variability of each spectrum can be accounted for by a linear combination of the first and second principal components with scores, shown in (b) in two-dimensional space. This presentation depicts the clustering of the data set and thus represents the different conformational states of PLL. Particularly, the clusters 2 and 4 (light and dark green) are the one group attributed to $\alpha$-helix, whereas the third cluster is the group attributed to the $\beta$-sheet state, and first – a mixture of both $\alpha$-helix and $\beta$-sheet.

in Figure S8 in the Supporting Information. However, we would like to note that no preprocessing is in fact necessary for the PCA to capture the physical information.

The second principal component on the other hand exhibits pronounced spectral features, most notably at the vibrational frequencies of the $\alpha$-helix and $\beta$-sheet states at 1644 and 1618 $cm^{-1}$, respectively. On first sight, it is counterintuitive that both features are present in this component. However, one has to keep in mind that this component is a correction term to the shifted *average* experimental spectrum and is the same for all experimental spectra; only the scores will be different. As the average spectrum has both features for the $\alpha$-helical and $\beta$-sheet states, the scores of $PC_2$ for each spectrum correct the average according to the secondary structure of the PLL for the corresponding measurement step. The fact that $PC_2$ has two features of opposite sign underlines this interpretation. For example, to reconstruct the spectrum of the $\alpha$-helical state the average needs to be corrected by $PC_2$ with positive score and with negative score for a predominantly $\beta$-sheet state. We thus conclude that the second principal component and its scores contain the information about the secondary structure of the molecules. Therefore, the scores of $PC_2$ can be used to cluster the data to different conformational states.

In order to depict the results of all 200 experimentally obtained spectra, we plot the scores of $PC_1$ and $PC_2$ in Figure 4b against one another. The data points are color-coded according to the four distinct data sets of 50 spectra each. The four measurements sets can be clearly distinguished in the plot as they form strongly correlated and nonoverlapping clusters. Directly after functionalization, the spectra are characterized by scores of $PC_2$ around zero, indicating that both conformational states of the molecules are present. After the first pD-jump the scores of $PC_2$ are strongly positive, which indicates that the polypeptides have undergone a structural change to a near unity $\alpha$-helix state distribution. Addition of SDS leads to spectra which are characterized by strongly negative scores of $PC_2$. This behavior implies that a clear structural transition from the $\alpha$-helix to the $\beta$-sheet state occurred. After the final pD-jump the spectra are again characterized by positive scores of $PC_2$, indicative of predominantly $\alpha$-helix state distribution. The $\alpha$-helix and $\beta$-sheet state distributions are very well separated and can be clearly distinguished. The two $\alpha$-helix state distributions are very similar, yet not identical with respect to their score values. As mentioned above, we ascribe these differences to incomplete structural transitions between the different states which lead to different distributions. As discussed earlier, the scores of $PC_1$ do most likely not contain information about the folding dynamics. However, even when disregarding this value, the data points still form distinct clusters well separated along the respective $k_{i,2}$ value distribution.

The measurements shown in Figure 3 and principal component analysis depicted in Figure 4 thus very clearly validate our concept of in vitro monitoring of the conformational changes of polypeptide monolayers using resonant surface enhanced infrared spectroscopy with plasmonic nanoantennas. We can reliably track the conformational changes of a monolayer of poly-L-lysine bound to the surface of resonant nanoantennas. Our results of PCA also reveal that the expected full conversion between the two conformational states does not take place and part of the molecules remain in the $\alpha$-helical state, while others are pushed into the $\beta$-sheet conformation, which is in fact a testament to our analysis technique.

In conclusion, we have demonstrated in vitro observation and tracking of conformational changes of a PLL monolayer (approximately 1600 molecules per antenna) with the help of resonant surface enhanced infrared absorption spectroscopy and principal component analysis. By binding the PLL molecules to the gold nanoantenna, we certify that secondary structure changes of one protein monolayer can take place reversibly. We believe that with further advances it will be possible to scale the process to a few or single nanoantennas or even proteins and observe the conformational behavior of individual entities. In order to achieve this goal, improvements of infrared light sources, e.g., the development of brilliant broadband laser sources,[53,54] and advanced nanoantenna designs[55] are needed. Moreover, selective placement based on tailored functionalization schemes and electron beam lithography is important, which has already been demonstrated for other systems and should be transferable to our situation.[38] In the future, integrated chip-level technology for biological and even medical applications and for point-of-care testing of biosamples in minor amounts would tremendously benefit


DOI: 10.1021/acs.nanolett.8b02372
Nano Lett. 2019, 19, 1–7

neurodegenerative patients and an aging population, as protein misfolding is believed to be at the root of these diseases.

## ■ ASSOCIATED CONTENT

### Supporting Information

The Supporting Information is available free of charge on the ACS Publications website at DOI: 10.1021/acs.nanolett.8b02372.

Figures of fluidic cells used for the in vitro measurements, details regarding FTIR measurements and functionalization procedures, reference IR and CD measurements, results of PLL folding for different antenna length, details concerning PCA analysis (PDF)

## ■ AUTHOR INFORMATION


### Corresponding Author

*E-mail: neubrech@kip.uni-heidelberg.de.

### ORCID

Rostyslav Semenyshyn: 0000-0001-6818-7500

Frank Neubrech: 0000-0002-5437-4118


### Notes

The authors declare no competing financial interest.

## ■ ACKNOWLEDGMENTS

We thank Sara Weirich (Institute of Biochemistry, University of Stuttgart) for circular dichroism measurements. The authors gratefully acknowledge financial support by the ERC Advanced Grant (COMPLEXPLAS), Deutsche Forschungsgemeinschaft (SPP1391), Baden-Württemberg Stiftung (PROTEINSENS), MWK Baden-Württemberg (IQST), Max Planck Society, and BMBF (03IS2101E). C.P. thanks the Deutsche Forschungsgemeinschaft (DFG) for funding (Heisenberg fellowship, project number: 286735196).

## ■ REFERENCES


(1) Knowles, T. P. J.; Vendruscolo, M.; Dobson, C. M. *Nat. Rev. Mol. Cell Biol.* **2014**, *15* (7), 384−396.

(2) Irwin, D. J.; Lee, V. M.-Y.; Trojanowski, J. Q. *Nat. Rev. Neurosci.* **2013**, *14* (9), 626−636.

(3) Kelly, S. M.; Jess, T. J.; Price, N. C. *Biochim. Biophys. Acta, Proteins Proteomics* **2005**, *1751* (2), 119−139.

(4) Greenfield, N. J. *Nat. Protoc.* **2006**, *1* (6), 2876−2890.

(5) Wüthrich, K. *J. Biol. Chem.* **1990**, *265* (36), 22059−22062.

(6) Clore, G. M.; Gronenborn, A. M. *Science* **1991**, *252* (5011), 1390−1399.

(7) Aslam, N.; Pfender, M.; Neumann, P.; Reuter, R.; Zappe, A.; Oliveira, F. F. De; Denisenko, A.; Onoda, S.; Isoya, J.; Wrachtrup, J. *Science* **2017**, *357* (6346), 67−71.

(8) Boutet, S.; Lomb, L.; Williams, G. J.; Barends, T. R. M.; Aquila, A.; Doak, R. B.; Weierstall, U.; DePonte, D. P.; Steinbrener, J.; Shoeman, R. L.; et al. *Science* **2012**, *337*, 362−364.

(9) Schotte, F.; Lim, M.; Jackson, T. A.; Smirnov, A. V.; Soman, J.; Olson, J. S.; Phillips, G. N. J.; Wulff, M.; Anfinrud, P. A. *Science* **2003**, *300* (5627), 1944−1947.

(10) Ruggeri, F. S.; Adamcik, J.; Jeong, J. S.; Lashuel, H. A.; Mezzenga, R.; Dietler, G. *Angew. Chem., Int. Ed.* **2015**, *54* (8), 2462−2466.

(11) Amenabar, I.; Poly, S.; Nuansing, W.; Hubrich, E. H.; Govyadinov, A. A.; Huth, F.; Krutokhvostov, R.; Zhang, L.; Knez, M.; Heberle, J.; et al. *Nat. Commun.* **2013**, *4*, 2890.

(12) Si, W.; Aksimentiev, A. *ACS Nano* **2017**, *11*, 7091.

(13) Barth, A. *Biochim. Biophys. Acta, Bioenerg.* **2007**, *1767* (9), 1073−1101.

(14) Lippert, J. L.; Tyminski, D.; Desmeules, P. J. *J. Am. Chem. Soc.* **1976**, *98* (22), 7075−7080.

(15) Barth, A.; Haris, P. I. *Biological and Biomedical Infrared Spectroscopy*; IOS Press: Amsterdam, 2009.

(16) Dousseau, F.; Pézolet, M. *Biochemistry* **1990**, *29*, 8771−8779.

(17) Venyaminov, S. Y.; Kalnin, N. N. *Biopolymers* **1990**, *30*, 1259−1271.

(18) Dzwolak, W.; Smirnovas, V. *Biophys. Chem.* **2005**, *115*, 49−54.

(19) Dzwolak, W.; Muraki, T.; Kato, M.; Taniguchi, Y. *Biopolymers* **2004**, *73*, 463−469.

(20) Deflores, L. P.; Ganim, Z.; Nicodemus, R. A.; Tokmakoff, A. *J. Am. Chem. Soc.* **2009**, *131*, 3385−3391.

(21) Ataka, K.; Stripp, S. T.; Heberle, J. *Biochim. Biophys. Acta, Biomembr.* **2013**, *1828* (10), 2283−2293.

(22) Fallah, M. A.; Stanglmair, C.; Pacholski, C.; Hauser, K. *Langmuir* **2016**, *32*, 7356−7364.

(23) Baumann, A.; Kerruth, S.; Fitter, J.; Büldt, G.; Heberle, J.; Schlesinger, R.; Ataka, K. *PLoS One* **2016**, *11* (3), e0151051.

(24) Neubrech, F.; Huck, C.; Weber, K.; Pucci, A.; Giessen, H. *Chem. Rev.* **2017**, *117*, 5110−5145.

(25) Cerjan, B.; Yang, X.; Nordlander, P.; Halas, N. J. *ACS Photonics* **2016**, *3* (3), 354−360.

(26) Huck, C.; Neubrech, F.; Vogt, J.; Toma, A.; Gerbert, D.; Katzmann, J.; Härtling, T.; Pucci, A. *ACS Nano* **2014**, *8* (5), 4908−4914.

(27) Brown, L. V.; Yang, X.; Zhao, K.; Zheng, B. Y.; Nordlander, P.; Halas, N. J. *Nano Lett.* **2015**, *15* (2), 1272−1280.

(28) Neubrech, F.; Pucci, A.; Cornelius, T. W.; Karim, S.; García-Etxarri, A.; Aizpurua, J. *Phys. Rev. Lett.* **2008**, *101*, 157403.

(29) Zhang, Y.; Zhen, Y.-R.; Neumann, O.; Day, J. K.; Nordlander, P.; Halas, N. J. *Nat. Commun.* **2014**, *5*, 4424.

(30) Adato, R.; Yanik, A. A.; Amsden, J. J.; Kaplan, D. L.; Omenetto, F. G.; Hong, M. K.; Erramilli, S.; Altug, H. *Proc. Natl. Acad. Sci. U. S. A.* **2009**, *106*, 19227−19232.

(31) Anker, J. N.; Hall, W. P.; Lyandres, O.; Shah, N. C.; Zhao, J.; Van Duyne, R. P. *Nat. Mater.* **2008**, *7*, 442−453.

(32) Rodrigo, D.; Limaj, O.; Janner, D.; Etezadi, D.; Javier García De Abajo, F.; Pruneri, V.; Altug, H. *Science* **2015**, *349* (6244), 165−168.

(33) Wu, C.; Khanikaev, A. B.; Adato, R.; Arju, N.; Yanik, A. A.; Altug, H.; Shvets, G. *Nat. Mater.* **2012**, *11* (1), 69−75.

(34) Ament, I.; Prasad, J.; Henkel, A.; Schmachtel, S.; Sönnichsen, C. *Nano Lett.* **2012**, *12* (2), 1092−1095.

(35) Adato, R.; Altug, H. *Nat. Commun.* **2013**, *4*, 2154.

(36) Limaj, O.; Etezadi, D.; Wittenberg, N. J.; Rodrigo, D.; Yoo, D.; Oh, S. H.; Altug, H. *Nano Lett.* **2016**, *16* (2), 1502−1508.

(37) Etezadi, D.; Warner, J. B.; Lashuel, H. A.; Altug, H. *ACS Sensors* **2018**, *3* (6), 1109−1117.

(38) Dregely, D.; Neubrech, F.; Duan, H.; Vogelgesang, R.; Giessen, H. *Nat. Commun.* **2013**, *4*, 2237.

(39) Etezadi, D.; Warner, J. B.; Ruggeri, F. S.; Dietler, G.; Lashuel, H. A.; Altug, H. *Light: Sci. Appl.* **2017**, *6*, e17029.

(40) Myer, Y. P. *Macromolecules* **1969**, *2* (6), 624−628.

(41) Seipke, G.; Arfmann, H.; Wagner, K. G. *Biopolymers* **1974**, *13*, 1621−1633.

(42) Shepherd, I. W. *Biochem. J.* **1976**, *155* (3), 543−548.

(43) Wang, Y.; Chang, Y. C. *Macromolecules* **2003**, *36* (17), 6511−6518.

(44) Satake, I.; Yang, J. T. *Biochem. Biophys. Res. Commun.* **1973**, *54* (3), 930−936.

(45) Barth, A.; Zscherp, C. *Q. Rev. Biophys.* **2002**, *35* (4), 369−430.

(46) Neubrech, F.; Beck, S.; Glaser, T.; Hentschel, M.; Giessen, H.; Pucci, A. *ACS Nano* **2014**, *8* (6), 6250−6258.

(47) Eilers, P. H. C. *Anal. Chem.* **2003**, *75* (14), 3631−3636.

(48) D'Andrea, C.; Bochterle, J.; Toma, A.; Huck, C.; Neubrech, F.; Messina, E.; Fazio, B.; Maragò, O. M.; Di Fabrizio, E.; Lamy De La Chapelle, M.; et al. *ACS Nano* **2013**, *7* (4), 3522−3531.

(49) Chittchang, M.; Salamat-Miller, N.; Alur, H. H.; Velde, D. G. V.; Mitra, A. K.; Johnston, T. P. J. *J. Pharm. Pharmacol.* **2002**, *54* (11), 1497−1505.




DOI: 10.1021/acs.nanolett.8b02372
*Nano Lett.* 2019, 19, 1−7

(50) Erickson, H. P. *Biol. Proced. Online* **2009**, *11* (1), 32−51.
(51) Wagner, M. S.; Castner, D. G. *Langmuir* **2001**, *17*, 4649−4660.
(52) Pribić, R. Principal Component Analysis of Fourier Transform Infrared And/or Circular Dichroism Spectra of Proteins Applied in a Calibration of Protein Secondary Structure And/or Circular Dichroism Spectra of Proteins Applied in a Calibration of Protein Secondary St. *Anal. Biochem.* **1994**, *223*, 26−34.
(53) Steinle, T.; Mörz, F.; Steinmann, A.; Giessen, H. *Opt. Lett.* **2016**, *41* (21), 4863−4866.
(54) Mörz, F.; Semenyshyn, R.; Steinle, T.; Neubrech, F.; Zschieschang, U.; Klauk, H.; Steinmann, A.; Giessen, H. *Opt. Express* **2017**, *25* (26), 32355.
(55) Dong, L.; Yang, X.; Zhang, C.; Cerjan, B.; Zhou, L.; Tseng, M. L.; Zhang, Y.; Alabastri, A.; Nordlander, P.; Halas, N. J. *Nano Lett.* **2017**, *17*, 5768−5774.



DOI: 10.1021/acs.nanolett.8b02372
*Nano Lett.* 2019, 19, 1−7